Reversible association and network formation in 3 : 1 ligand–metal polymer solutions†

Shihu Wang, Chun-Chung Chen and Elena E. Dormidontova*

Received 19th February 2008, Accepted 28th May 2008
First published as an Advance Article on the web 31st July 2008
DOI: 10.1039/b802839g

Formation of reversible metallo-supramolecular networks based on 3 : 1 ligand–metal complexes between end-functionalized oligomers and metal ions was studied using Monte Carlo simulations. The fraction of 1 : 1, 2 : 1 and 3 : 1 ligand–metal complexes was obtained and analyzed using an analytical approach as a function of oligomer concentration, c and metal-to-oligomer ratio, r. At low concentration the maximum in the number-average molecular weight is achieved near the stoichiometric composition ($r = 2/3$), while the weight-average molecular weight maximum is shifted to higher r ($\simeq 0.75$). With an increase in oligomer concentration the molecular weight maxima shift to higher metal-to-oligomer ratios (similar to the experimentally observed viscosity) due to diminished ring formation. Network formation as determined from the analysis of the molecular weight distribution and reduced average cluster size occurs in a limited range of metal-to-oligomer ratios at sufficiently large oligomer concentrations. At oligomer concentrations slightly exceeding the onset of network formation its growth occurs by means of incorporation of sol molecules into the dangling parts of the network. In the range of r close to the stoichiometric composition the overall number of oligomers in the sol and dangling parts is found to remain nearly constant as a function of oligomer concentration and equal to that at the onset of network formation. The average molecular weight between effective crosslinks decreases with oligomer concentration and reaches its minimum at the stoichiometric composition, where the high-frequency elastic plateau modulus approaches its maximal value. At high oligomer concentrations the plateau modulus follows a $c^{1.8}$ concentration dependence, similar to recent experimental results for metallo-supramolecular networks.

1 Introduction

Supramolecular polymers[1–3] have attracted considerable interest during the past decade for their exceptional self-healing properties based on noncovalent interactions and a wide range of potential applications. We focus in this contribution on metallo-supramolecular networks in which the reversible bonds between monomeric units are based on metal–ligand coordinative interactions.[4–11] Versatile metallo-supramolecular networks have been synthesized with various mechanical, chemical and stimuli-responsive properties that can be easily tailored by fine-tuning the molecular architecture, thermodynamic and kinetic stability by choosing appropriate metal–ligand pairs.[2,4,12] The rational design of the supramolecular networks requires a full understanding and exploration of the underlying interconnection between molecular components and the resulting bulk material's properties.[9,13] Despite the considerable interest in metallo-supramolecular polymers, physical characterization and experimental analysis of their properties are still in an early stage of development (due to the complexity of the system and difficulty in experimental measurements caused by the intrinsic kinetic lability of the coordinative interactions) with only a few experimental studies capable of elucidating their properties at a microscopic level.[5,6,8,9,11] Using a model that captures the essential characteristics of the formation of supramolecular polymers, computer simulation and theoretical modeling represent highly efficient tools to investigate the microscopic details and analyze the underlying mechanism of different processes without perturbing the equilibrium state. In this paper using a combined computer simulation and theoretical modeling approach, we study metallo-supramolecular polymers in solutions containing end-functionalized linear flexible oligomers and lanthanide-like metal ions as shown in Fig. 1. The lanthanide metal ions can form complexes with up to three tridentate ligands leading to the formation of tris (3 : 1) ligand–metal complexes and are therefore capable of forming metallo-supramolecular networks. In this paper the mechanism of the self-assembly of metallo-supramolecular polymers and properties of the formed network are analyzed in detail in order to provide a fundamental understanding of the process which can be useful in guiding further experimental characterization and synthetic efforts to engineer materials with desired properties.

The formation of metallo-supramolecular polymers in aqueous solution in the presence of bifunctional ligands and lanthanide metal ions was investigated recently by Vermonden and coworkers.[5,6] These groups employed water soluble 2,6-dicarboxypyridine ligands with lanthanide metal ions, *i.e.*

Department of Macromolecular Science and Engineering, Case Western Reserve University, Cleveland, Ohio, USA. E-mail: eed@case.edu

† Electronic supplementary information (ESI) available: Composition dependence of the average number fraction of different species at several metal-to-oligomer ratios, determination of the onset of reversible network formation from the molecular weight distribution and mesh size calculations. See DOI: 10.1039/b802839g

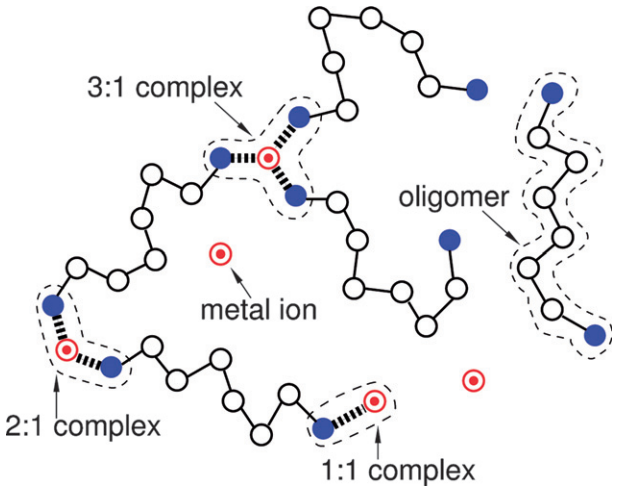

Fig. 1 A schematic representation of metallo-supramolecular polymers.

neodymium(III) or lanthanum(III), to produce thermo-reversible metallo-supramolecular networks. At a critical oligomer concentration or metal-to-oligomer ratio these materials exhibit a sharp increase in the reduced viscosity during the sol–network transition.[5] The rheological studies reveal that at high oligomer concentrations the supramolecular network yields a high viscosity and viscoelastic properties which can be described with the Maxwell model.[6] For one of the oligomers studied the results agree well with the prediction of Cates and Candau's model[14] that describes the dynamics of linear equilibrium polymers, indicating that only a few 3 : 1 ligand–metal crosslinks exist in this supramolecular network. At the same time metallo-supramolecular networks formed from a different oligomer possess a smaller molecular weight between effective crosslinks and viscoelastic behavior that follows a $c^{1.8}$ concentration scaling for the high-frequency elastic plateau modulus which is similar to what was observed in branched worm-like CTAB (hexadecyltrimethylammonium bromide) micelles (in the presence of high concentration of salt).[15] Comparisons with some of the results of these studies[5,6] will be made throughout the paper. A more complex system involving both lanthanide and transition metal ions and the tridentate bis[2,6-bis(1′-methylbenzimidazolyl)-4-hydroxypyridine] (HO-BIP) ligand was recently utilized by Rowan and coworkers[4,7,16] to obtain a metallo-supramolecular network. The resulting network demonstrates multiple stimuli-responsive behavior, including thermo-, chemo- mechano- and photo-responses, the nature of which can be controlled by the combination of transition and lanthanide metal ions and different solvents.[8] Evidently the behavior of such a network is far more complex due to the presence of two types of metal ions, phase separation, crystallization, colloidal network formation and so on.[8] From a modeling perspective, to understand the behavior of such a complex system would require a more sophisticated model, which can be built based on the results of a more general approach such as the one discussed below. Besides the systems with lanthanide metal ions, there are some recent reports by Sijbesma and coworkers on the synthesis of coordination polymers of high molecular weight due to network formation from bifunctional phosphorus ligands and transition metal ions palladium(II) or platinum(II) in a similar 3 : 1 ligand-to-metal stoichiometry.[17] More recently, the same group found that combining diphenylphosphinite telechelic polytetrahydrofuran with either rhodium(I) or iridium(I) chloride in chloroform with a ligand-to-metal stoichiometry of 4 : 1 also leads to the formation of mechano-reversible metallo-supramolecular networks.[18] It is also worthwhile to mention systems where network formation occurs *via* dimerization of quadruple hydrogen-bonding ureido-pyrimidone units between end-functional oligomers and trifunctional units.[19,20] Unfortunately these studies do not provide a large body of experimental data which can be used for comparison with our results. Other types of metallo-supramolecular networks include networks formed by 2 : 1 complexes between transition metal ions and ligands being part of side-chains of long (comb-like) polymers.[11,21–24] The self-complementary or complementary hydrogen-bonding interactions are also widely used to construct supramolecular networks by adopting similar approaches.[25] While these supramolecular networks are also reversible, their behavior should be described by the models of network formation in polymer chains with multiple stickers along the chain rather than the model discussed below.

Irreversible gel formation by telechelic prepolymers and multifunctional crosslinkers has been investigated using computer simulations.[26–29] The structural statistics of various types of network imperfections and the cycle ranks of the networks were studied by Eichinger and coworkers,[26,27] varying the ratios between trifunctional crosslinkers and end-linked elastomers. Using Monte Carlo simulations Panagiotopoulos and coworkers studied the formation and structural properties of end-linked polymer networks, varying the chain length as well as the ratio between tetrafunctional crosslinker and prepolymer chain ends.[28] The sol fraction and the number of loops and pendent structures were evaluated and it was found that the gel with a minimum of soluble fraction and maximum fraction of elastic material is formed at a non-stoichiometric composition, which increases with increasing precursor polymer chain length.[28] These computational studies, while having an evident similarity to the case considered here, deal either with irreversible or reversible network formation without consideration of non-equal reactivity and cooperativity of complexation, which are important for metallo-supramolecular network formation. There are also many simulation studies which consider reversible network formation, either between telechelic polymers where crosslinking occurs by the association of an unlimited number of chain ends[30,31] or by binary reversible association among multiple stickers along the chain. In both cases the intra-molecular association and the mechanism of network formation can be quite different from that considered here. While different simulation techniques have been developed to study gelation, little effort has been devoted to studying the formation of supramolecular polymers through metal–ligand complexation.[32] To the best of our knowledge, this is the first study devoted to modeling the formation of metallo-supramolecular networks.

A successful representation of the formation of metallo-supramolecular networks by an analytical model would require the consideration of the following factors: reversibility of binding, unequal reactivity and cooperativity of the first, second and third ligand–metal bonds and should account for formation of both inter- as well as intra- molecular bonds. The first shell substitution (*i.e.* cooperativity) effects coupled with cyclization

has been considered in analytical models by Gordon and Scantlebury[33] and later by Macosko and coworkers for the acid-catalyzed sol–gel polymerization with the kinetic-recursive (KR) model, accounting for up to two-membered rings.[34] A good agreement between the KR model and Monte Carlo simulations (in terms of degree of polymerization) has been achieved in the pre-gel region. However, near the gel point discrepancies between the KR model and an exact Monte Carlo model arose and the KR model could not predict the experimentally observed gel conversions. Another model that considered both smallest ring formation and different intrinsic reactivity was utilized by Sarmoria and coworkers to study the stepwise copolymerization between trifunctional and bifunctional monomers.[35] Both parameters delay the gel point when considered individually but either reinforce or compensate each other depending on the reacting conditions when present simultaneously. A satisfactory comparison was made between the predictions of this model and the experimental gel point. However, this model described irreversible stepwise reactions with no substitution effect and formation of only the smallest possible rings was considered. There are also many other models that have been put forward to describe different aspects of gel formation, starting from the classical Flory–Stockmayer model,[36–38] the rate and kinetic theory by Gordon and Scantlebury,[33] and lattice models,[39] to models that consider effects of different factors on gelation: unequal reactivity,[40] ring formation[39,41–43] as well as substitution effects.[44] However, we are not aware of any model that can be directly applied or modified easily to be applicable to the formation of metallo-supramolecular networks. We hope that our simulation results will be helpful in the development of an appropriate analytical model in the future.

In our computer simulation model discussed below we will consider reversible (*i.e.* kinetically labile) metal–ligand complexation, taking into account different binding energies for the formation of the first, second and third bond between the metal ion and ligands with no preference for any particular molecular architectures. Using this model, we will discuss the effect of oligomer concentration and metal-to-oligomer ratio on the properties of the metallo-supramolecular polymers. The conditions for the formation of a metallo-supramolecular network will be determined. Then the network properties will be addressed in detail by investigating the sol, network, dangling parts, molecular weight between effective crosslinks and high-frequency elastic plateau modulus. We will compare our results with existing experimental data and make predictions regarding the mechanism of network formation, as well as the influence of oligomer concentration and metal-to-oligomer ratio on the properties of metallo-supramolecular networks.

2 Computational details

We employ Monte Carlo (MC) simulations using the bond fluctuation model (BFM)[45,46] to study the reversible formation of metallo-supramolecular networks by end-functionalized oligomers *via* ligand–metal ion complexation. In our simulations, a linear flexible oligomer consists of 8 covalently bonded monomers, 6 of which represent a spacer and the two terminal monomers are ligands. The metal ion is modeled as a monomer capable of reversible association with up to three ligands. We do not consider the influence of electrostatic interactions (or counterion distribution) on the properties of the supramolecular polymers, as we are interested in solutions of supramolecular polymers with salt-screened electrostatic interactions. Each simulation configuration consists of a fixed number N_o of oligomers and N_m of metal ions. We note that the spacer segments in the oligomers are considered to be flexible, *i.e.* there is no penalty for bending a covalent bond of the spacer. We also neglect any penalty for bending reversible bonds between metal ions and ligands. This model is designed to address coordination bond formation between lanthanide metal ions and ligands,[47] which was a subject of intensive experimental studies in the recent decade.[4–6,8] In accordance with BFM rules, the distance between any two covalently bonded monomers (or reversibly bonded ligands and metal ions) is limited to the following values $2a,\sqrt{5}a,\sqrt{6}a,\sqrt{7}a,3a,\sqrt{10}a$ and each monomer occupies an effective volume of $8a^3$ (with a being the unit spacing of the cubic lattice). This allows us to take into account the excluded volume of polymers, so that our results represent good solvent conditions. We note that the oligomer concentrations discussed below are in terms of the number of oligomers per unit volume and are presented in units of a^{-3}. To minimize any boundary effects, we use a periodic cubic lattice of size $(64a)^3$.

Formation of the first bond between a metal ion and a ligand results in a mono (1 : 1) ligand–metal complexation, which lowers the energy of the system by $\Delta E_1 = 13kT$ (where k is the Boltzmann constant and T is the temperature). The mono (1 : 1) ligand–metal complex can form a reversible bond with another ligand and become a bis (2 : 1) ligand–metal complex, resulting in an additional energy decrease by $\Delta E_2 = 9kT$. Finally, the formation of the third bond between a metal ion in a bis (2 : 1) ligand–metal complex and a ligand leads to a tris (3 : 1) ligand–metal complex, which is accompanied by a further energy decrease by $\Delta E_3 = 7kT$. The association energies we use in our simulation were chosen to reproduce the equilibrium constants K_i for complexation between the lanthanum metal ion La^{3+} ($\log K_1 = 7.98$, $\log K_2 = 5.81$, $\log K_3 = 4.27$) and the dipicolinate ion.[48] Other metal ions from the lanthanide series may have somewhat different association constants, which would depend on the ligand, solvent and counterions. Nonetheless, we believe that the results presented below expose the qualitative (and quantitative) features common for any supramolecular complex involving lanthanide ions, as will be discussed below.

Following the standard BFM procedure, the configuration of the system is updated by randomly selecting one monomer and attempting its move (following the Metropolis algorithm) to a randomly chosen nearest-neighboring site. The move is rejected if it violates the space constraints described above. In each MC update, the reversible bonds between metal ions and ligands are treated in the same way as the covalent bonds. In order to take into account reversible association, additional bonding updates are performed following the moving attempts of ligands. After the moving attempt of the ligand, a reversible bond is assumed to be broken if the ligand was previously bonded to a metal ion. All metal ions within the bonding distance from the ligand and capable of forming bonds with it are checked and a new reversible bond is chosen from all the possible ones with a probability given by their respective Boltzmann weights $C\exp(\Delta E_i/kT)$, where ΔE_i is the energy change of the system for the formation of

the new bond [$i = 1$, 2 or 3 for reversible bond leading to mono (1 : 1), bis (1 : 2) or tris (1 : 3) ligand–metal complex formation, respectively] and $C = \left[1 + \sum_{i=1}^{3} \sum_{j=1}^{N_{a_i}} \exp(\Delta E_i/kT)\right]^{-1}$ being the probability of not forming a bond (N_{a_i} is the total number of available bonding sites for the bond of type i for this ligand). Depending on its Boltzmann weight, the old bond is kept or a new one is formed or no reversible bond is formed after the bonding update. We disregard the effect of distance on the respective Boltzmann weights. We note that this method of bonding update is different from the commonly used Metropolis algorithm but it also satisfies detailed balance. As the new bonding configuration of the system is directly drawn from the Boltzmann probability distribution, the association–dissociation events proceed with a minimal potential barrier resulting in a fast equilibration for reversible association.[49]

A Monte Carlo time step (MCts) is defined as the number of MC updates equal to the number of monomers (including oligomers and metal ions) in the system. It corresponds to the simulation time during which each monomer has a chance to make one moving attempt on average. The system is brought to equilibrium through the MC algorithm after a series of random updates of no less than $2^{23} \approx 8.4 \times 10^6$ MCts. All measurements are performed by averaging over $2^{22} \approx 4.2 \times 10^6$ subsequent simulation configurations.

3 Results and discussion

3.1 Fraction of mono (1 : 1), bis (2 : 1) and tris (3 : 1) ligand–metal complexes

As stated above, the reversible association between ligands and metal ions leads to the formation of different ligand–metal complexes. The fractions of mono (1 : 1), bis (2 : 1), and tris (3 : 1) ligand–metal complexes with respect to the total number of metal ions calculated from the simulations are referred to as m_1, m_2, and m_3 in the following. The fraction of free metal ions is then $m_0 = 1 - m_1 - m_2 - m_3$ and similarly the fraction of the occupied ligands with respect to total number of ligands is $f_l = 0.5(m_1 + 2m_2 + 3m_3)r$, where $r = N_m/N_o$ is the metal-to-oligomer ratio (N_m and N_o are number of metal ions and oligomers in the system, respectively). The dependence of the fraction of occupied ligands on the metal-to-oligomer ratio at fixed oligomer concentrations is found to be similar to the results of isothermal titration calorimetric experiments.[5] The fraction of occupied ligands linearly increases with metal content in the metal-poor region and reaches a saturation level corresponding to fully occupied ligands above the stoichiometric metal-to-oligomer ratio of $r = 2/3$ (*i.e.* one metal per three ligands) independent of oligomer concentration.

To describe the metal–ligand association analytically, we apply a simple model based on the chemical-equilibrium among different ligand–metal complexes, using a similar approach to that applied to study 2 : 1 ligand–metal complexes:[13,32,50,51]

$$K_i m_{i-1}[2N_o - N_m(m_1 + 2m_2 + 3m_3)]\frac{v}{V} = m_i \qquad (1)$$

where $K_i = \exp(\Delta E_i/kT - \Delta S_i/k)$ is the equilibrium constant for the formation of mono ($i = 1$), bis ($i = 2$) and tris ($i = 3$) ligand–metal complexes; ΔE_i is the energy of binding and ΔS_i is the entropic penalty for the formation of the corresponding complexes, m_i is the fraction of the corresponding complexes, V is the total volume of the system and v is the reference volume [in the BFM the reference volume reflects the number of available sites for nearest-neighbors (v is about $54a^3$)].[52] Eqn 1 expresses the equilibrium (with equilibrium constant K_i) between the fraction of m_i and m_{i-1} complexes and concentration of free oligomers (expression in the square brackets multiplied by v/V). For the lanthanide metal ions considered here the coordination bonds are very mobile,[47] so the entropic penalty ΔS_i is due to excluded volume only. However, for other types of metal ions, such as transition metals where formation of either *cis*- and *trans*-isomers is strongly preferred (depending on ligand, solvent, *etc.*)[53] the entropic penalty for a coordination bond would also include the orientational specificity of association. We plan to consider this situation in our future work. Rearranging eqn 1 some simple relationships can be derived:

$$\frac{m_3}{m_2} = \frac{K_3}{K_2}\frac{m_2}{m_1} \qquad (2)$$

$$\frac{m_2}{m_1} = \frac{K_2}{K_1}\frac{m_1}{(1 - m_1 - m_2 - m_3)} \qquad (3)$$

$$K_3 m_2[2N_o - N_m(m_1 + 2m_2 + 3m_3)]\frac{v}{V} = m_3 \qquad (4)$$

The fraction of different ligand–metal complexes m_1, m_2, m_3 (and free metal ions m_0) can be calculated numerically by solving the equations above. As is discussed below, the analytical predictions match the simulation results quite well at sufficiently high oligomer concentrations ($N_o/V > 0.0002$ for all r). However, since the analytical model does not account for ring formation, some deviation may occur at lower oligomer concentrations where ring formation dominates.[32,51]

Metal-to-oligomer ratio dependence. The fraction of different ligand–metal complexes is shown in Fig. 2 (a) as a function of the metal-to-oligomer ratio, r, for a constant oligomer concentration. In the oligomer-rich region ($r < 0.6$) tris (3 : 1) ligand–metal complexes dominate reaching nearly 100% at high oligomer concentrations, due to the large ligand excess. There is only a small fraction of bis (2 : 1) and mono (1 : 1) ligand–metal complexes in this region.

When the metal-to-oligomer ratio becomes larger ($0.6 < r < 2.0$) the fraction of tris (3 : 1) ligand–metal complexes starts to decline giving rise to bis (2 : 1) ligand–metal complexes. In particular above the stoichiometric composition ($r = 2/3$) the fraction of occupied ligands approaches 1, so that above this composition there is an excess of metal sites leading to an increase in the number of bis (2 : 1) and mono (1 : 1) ligand–metal complexes. The fraction of bis (2 : 1) ligand–metal complexes reaches its maximum at $r = 1$, which corresponds to one metal per two ligands. Using the analytical model we can calculate the absolute value of m_2 and the metal-to-oligomer ratio corresponding to the maximum of bis (2 : 1) ligand–metal complexes. To this end one can take the first derivative of eqn 3 (after substitution of eqn 2 for m_1) with respect to metal-to-oligomer ratio and let $\partial m_2/\partial r = 0$ (assuming $\partial m_3/\partial r \neq 0$):

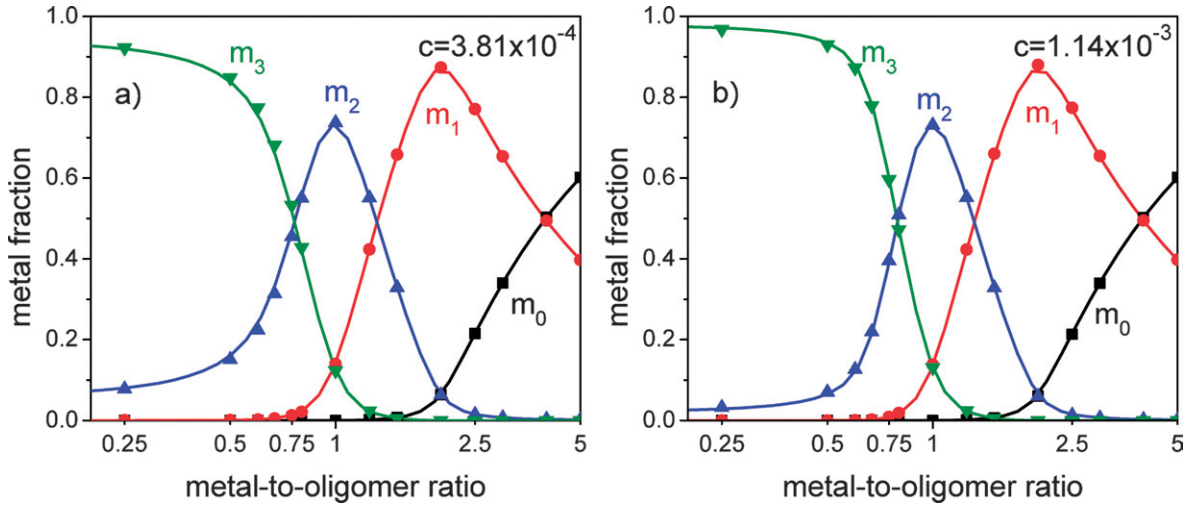

Fig. 2 The composition dependence of the mole fraction of metal ions in tris (3 : 1), m_3; bis (2 : 1), m_2; mono (1 : 1), m_1 ligand–metal complexes and free metal ions for two different oligomer concentrations (oligomers/volume, in units of a^{-3}) $c = 3.81 \times 10^{-4}$ (a) and $c = 1.14 \times 10^{-3}$ (b). Computer simulation data are shown as symbols whereas predictions of the analytical model are solid curves.

$$m_1 + 2m_2 + 3m_3 = 2 \quad (5)$$

This equation implies that at the maximum for m_2 on average two of the three metal ion sites are occupied. Solving this equation numerically together with eqn 2 and 3 one can find that at the maximum of bis (2 : 1) ligand–metal complexes $m_2^* \approx 0.733$, $m_3^* \approx 0.134$ and $m_1^* \approx 0.133$. Based on the analytical model m_1^*, m_2^* and m_3^* are independent of oligomer concentration.

Above $r = 1$, the fraction of bis (2 : 1) ligand–metal complexes starts to decrease as the imbalance between the number of ligands and metal sites becomes considerable leading to an increase in the mono (1 : 1) ligand–metal fraction. In its turn, the fraction of mono (1 : 1) ligand–metal complexes reaches its maximum at $r = 2$, *i.e.* when there is one metal site per ligand. Taking the first derivative of eqn 3 (after substitution of eqn 2 for m_3) with respect to the metal-to-oligomer ratio and letting $\partial m_1/\partial r = 0$ one can obtain (assuming $\partial m_2/\partial r \neq 0$) the following equation

$$m_1 + 2m_2 + 3m_3 = 1 \quad (6)$$

This equation implies that at the maximum for m_1 on average one of the three metal ion sites are occupied. Solving this equation numerically together with eqn 2 and 3 one can obtain $m_1' \approx 0.87$, $m_2' \approx 0.065$ and $m_3' \approx 1.61 \times 10^{-4}$ at the maximum of 1 : 1 ligand–metal fraction. The values of m_1', m_2' and m_3' predicted from the analytical model are independent of oligomer concentration. We note that these observations are based on derivations from the analytical model, which is valid at sufficiently high oligomer concentrations only. At low oligomer concentrations, when ring formation becomes predominant, some deviations from the predictions of the analytical model may occur (depending on K_i, metal-to-oligomer ratio, spacer length and rigidity).

When the metal-to-oligomer ratio becomes larger than 2 there is a large excess of metal ions in the system and the fraction of mono (1 : 1) ligand–metal complexes starts to decrease with an increase in the fraction of free metal ions. The fraction of bis (2 : 1) and tris (3 : 1) ligand–metal complexes is nearly zero in this region.

Oligomer concentration dependence. Comparing Fig. 2 (a) and (b), one can notice that oligomer concentration influences the fraction of different ligand–metal complexes mainly in the oligomer-rich region (below the stoichiometric composition, $r \lesssim 2/3$). In this region the fraction of tris (3 : 1) ligand–metal complexes steadily increases with oligomer concentration since the increase in the number of oligomers reduces the (translational) entropic penalty for bringing three ligands into the vicinity of each other. The increase in the fraction of tris (3 : 1) ligand–metal complexes is also accompanied by a decrease in the fractions of bis (2 : 1) [as well as mono (1 : 1)] ligand–metal complexes.

In the metal-rich region (above the stoichiometric composition) the fraction of different ligand–metal complexes does not change much with an increase in oligomer concentration [*cf.* Fig. 2 (a) and (b)]: the fraction of mono (1 : 1) ligand–metal complexes slightly increases while the fraction of bis (2 : 1) and tris (3 : 1) ligand–metal complexes slightly decreases. This change is very small, so that the fraction of different ligand–metal complexes when $m_1 = m_2$, $m_1 = m_3$ or at the maximum of 1 : 1 and 2 : 1 ligand–metal fractions is effectively independent of oligomer concentration, as discussed above. Our analytical model starts to deviate from the results of simulations at low oligomer concentration where ring formation, which was not considered in our model, becomes important. Due to ring formation, the increase in m_2^* (as well as a small decrease in m'_1) at low concentration is observed in simulations but is not predicted by the analytical model. Our simulations show that at very low concentrations ($N_o/V \leq 4 \times 10^{-5}$), the fraction of bis (2 : 1) ligand–metal complexes can reach nearly 1.0 at $r = 1$ when all associating species are rings (as discussed below) and it decreases to a somewhat smaller value ($m_2^* \approx 0.73$) at larger concentrations when small ring formation becomes less favorable (above $N_o/V \approx 3.74 \times 10^{-4}$ for $r = 1$) accompanied by an increase in

both fraction of the mono (1 : 1) and tris (3 : 1) ligand–metal complexes.

3.2 Smallest dominant species

As is discussed above, in the oligomer-rich region (3 : 1) tris ligand–metal complexes dominate on average, but what are the typical structures formed in this range? While analyzing the whole distribution is a rather complicated task, we looked more closely at small species,[26] which dominate the distribution at low oligomer concentrations and in the sol phase. The discussion presented below is based on our simulation results.

As shown in Fig. 3 for $N_o/V = 3.81 \times 10^{-4}$, when the metal-to-oligomer ratio is small, the dominant species are single unassociated oligomers. At $r = 0.3$ they comprise nearly 63.5% of the total number of species in the system, while the next most favorable species [containing tris (3 : 1) ligand–metal complexes] are the smallest ring with a side-chain (19.1%) and a mini-star composed of three oligomers (6.0%). The rest of the associated species comprise only 11%. With increasing metal content, the number fraction of single unassociated oligomers decreases greatly (to 31% for $r = 0.5$), indicating effective polymerization. The number fraction of the smallest rings with a side-chain increases (to 30%), while the third dominating species (7%) becomes the two smallest rings connected by an oligomer. The fraction of the rest of the associated species noticeably increases (to 33%). Around the stoichiometric composition ($0.6 < r < 0.8$) the dominant species becomes a smallest ring (27% at $r = 2/3$), which reflects the increase in the fraction of bis (2 : 1) ligand–metal complexes in this region (Fig. 2). The smallest ring with a side-chain and two smallest rings connected by an oligomer remain the next two most favorable species (23% and 13% correspondingly at $r = 2/3$). Contributions from other species further increase and reach their maximum value in the range ($0.6 < r < 0.8$) around the stoichiometric composition (36.7% for $N_o/V = 3.81 \times 10^{-4}$).

Further increases in the metal-to-oligomer ratio lead to an increase in the number fraction of the smallest rings, which reaches its maximum (contributing about 65% for $N_o/V = 3.81 \times 10^{-4}$) at $r = 1$ where 2 : 1 ligand–metal complexes dominate (Fig. 2). The next largest species is a ring composed of two oligomers (5.8% at $r = 1$). The number fraction of species with tris (3 : 1) ligand–metal complexes considerably decreases together with its largest representative, a smallest ring with a side-chain (3% at $r = 1$). This is consistent with the fact that the fraction of tris (3 : 1) ligand–metal complexes becomes negligibly small in this range of r values (Fig. 2). The number fraction of all other species decreases (to 26.5% at $r = 1$) with increasing metal content. In the metal-rich region ($r > 1.5$), single oligomers with each end occupied by one metal ion start to dominate the distribution (87% at $r = 2$ and nearly 100% at high metal content) because of the increase in the fraction of 1 : 1 ligand–metal complexes (Fig. 2). The other favorable species are linear chains composed of two oligomers (8.2% at $r = 2$) and the smallest rings (3.95% at $r = 2$), whose fractions decrease with an increase of the metal-to-oligomer ratio. The fraction of other species becomes considerably smaller as well.

3.3 Molecular weight

The molecular weight distribution as well as the weight- and number-average molecular weights, can be obtained by counting the number of supramolecular chains (or rings) N_i of molecular weight M_i.

Molecular weight distribution. The weight fraction molecular weight distribution obtained (averaging over $2^{22} \approx 4.2 \times 10^6$ MCts) at the stoichiometric composition for several oligomer concentrations is shown in Fig. 4. For small oligomer concentrations, the weight fraction decreases exponentially with molecular weight, *i.e.* $w_i \sim \exp(-\lambda M_i)$, where w_i is the weight fraction of species with a molecular weight M_i and λ is the decay constant. For the stoichiometric composition the decay constant λ decreases exponentially with oligomer concentration,

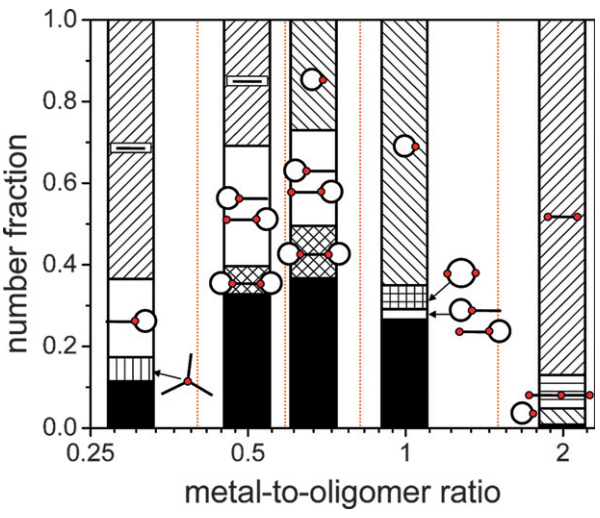

Fig. 3 The composition dependence of the average number fraction of the smallest dominant species (the three most favorable species are depicted) for the oligomer concentration $c = 3.81 \times 10^{-4}$.

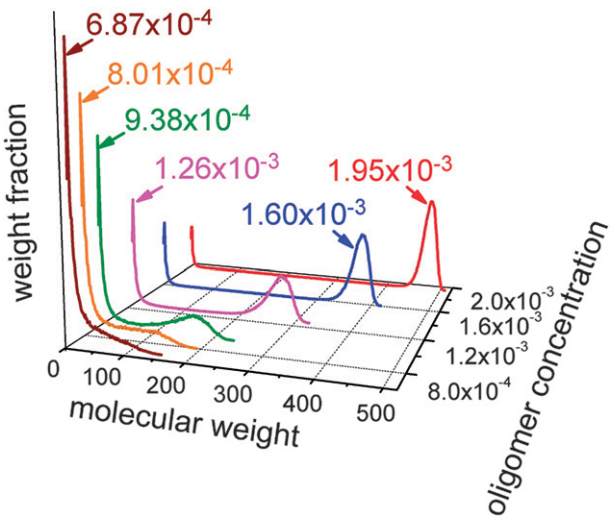

Fig. 4 The weight-average molecular weight distribution at the stoichiometric metal-to-oligomer ratio ($r = 0.67$) for several oligomer concentrations. The molecular weight is shown in units of oligomer molecular weight.

indicating a large increase in the average molecular weight.[36] At higher oligomer concentrations the molecular weight distribution starts to deviate from an exponential dependence developing a plateau at intermediate to large molecular weights. We note that the obtained distribution is a result of averaging over many MC steps. Each individual realization of the system may contain only a single large supramolecular chain (ring) or network being in equilibrium with several small species. Above a certain oligomer concentration (related to the onset of reversible network formation, as discussed below) the part of the distribution corresponding to large molecular weights starts to grow, developing a distinct peak, indicating the formation of large supramolecular objects. As is seen from Fig. 4 the peak becomes more narrow, its height increases and its position shifts linearly to higher values as the oligomer concentration increases (with the absolute values for the peak height and position being dependent on the simulation box size). Correspondingly the separation between the low and high molecular weight parts of the distribution increases and the contribution of the high molecular weight part steadily increases. The low molecular weight part of the distribution still follows the exponential dependence while the high-molecular weight part can be approximated by a (asymmetric) Gaussian or Lorenzian distribution. Analyzing the area under the corresponding parts of the distribution one can determine the sol and reversible network fraction, correspondingly (which will be discussed in detail below).

The average molecular weight distribution calculated at different metal-to-oligomer ratios (not shown) behaves rather similarly to that described above (and shown in Fig. 4). The only exception corresponds to the case of a strong mismatch in the number of oligomers and metal ions, when the distribution follows an exponential decay regardless of oligomer concentration.

Average molecular weight. The weight- and number-average molecular weights were calculated as $M_w = \Sigma N_i M_i^2 / \Sigma N_i M_i$ and $M_n = \Sigma N_i M_i / \Sigma N_i$, respectively. The results for M_w and M_n at different metal-to-oligomer ratios for several (low) oligomer concentrations are shown in Fig. 5.

For a constant oligomer concentration, the molecular weights (both number- and weight-average) reach large values when the metal-to-oligomer ratio r is between 0.5 and 1.0. In this range of metal-to-oligomer ratios, the fraction of both bis (2 : 1) and tris (3 : 1) ligand–metal complexes is considerable, implying a large degree of association leading to formation of high molecular weight supramolecular polymers (*cf.* the fraction of large species in Fig. 3). The mismatch between metal ions and ligands away from the stoichiometric composition will decrease the degree of association and thus the average molecular weight. Similar behavior based on viscosity measurements performed at constant polymer concentrations but with changing metal contents has been recently reported for aqueous solutions of Nd^{3+} (or La^{3+}) and bifunctional ligands consisting of two pyridine-2,6-dicarboxylate groups connected by a flexible spacer.[5] These supramolecular polymers exhibit high viscosity around the stoichiometric composition, which decreases quickly when there is an excess or deficiency of metal ions.

Even though both the number- and weight-average molecular weight reach large values in a similar range of metal-to-oligomer ratios (r), a close inspection shows that their maxima are attained at different r. Indeed, for sufficiently low oligomer concentrations the maximum of the number-average molecular weight occurs at about the stoichiometric composition $r \approx 2/3$, while the weight-average molecular weight reaches its maximum at about $r \approx 3/4$. We note that small rings involving 3 : 1 ligand–metal complexes also reach their maximum at the stoichiometric composition as is seen from Fig. 6. Since small rings are the dominant species at low oligomer concentrations, this maximum translates into the maximum of the number-average molecular weight. A slight excess in the number of metal ions makes possible ring-opening with the formation of larger molecular weight structures. This is the reason for the shift in the position of the maximum in M_w to larger r values, compared to the maximum in M_n. As is seen from Fig. 5, this trend persists over

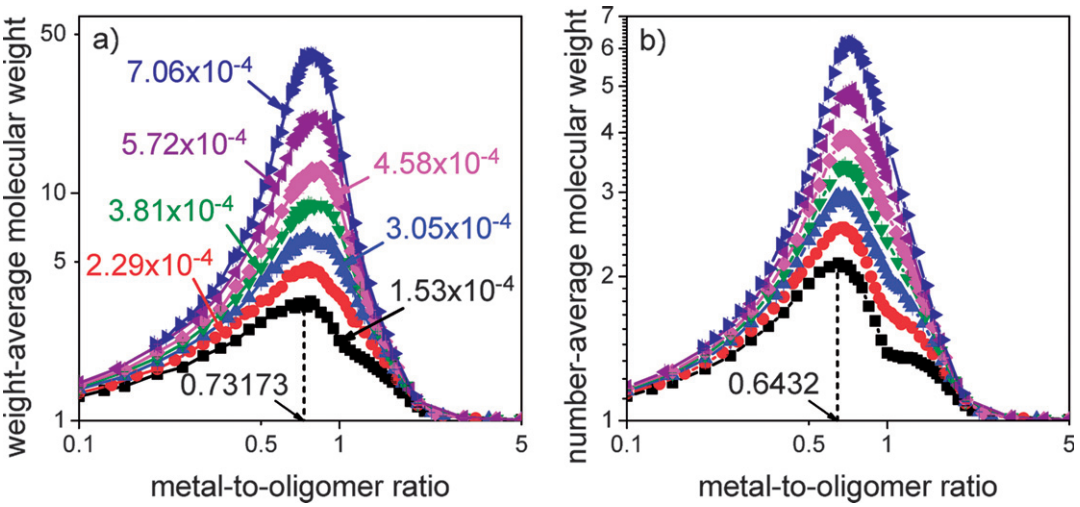

Fig. 5 The composition dependence of (a) weight- and (b) number-average molecular weights (in units of oligomer molecular weight) for different low oligomer concentrations [the same for (a) and (b)]. The vertical dashed lines correspond to the maximum of the weight- or number-average molecular weights for the lowest oligomer concentration considered.

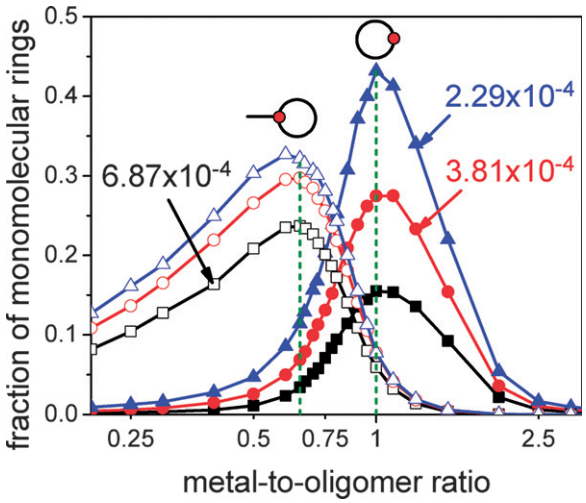

Fig. 6 The composition dependence of the smallest rings with bis (2 : 1) (solid) and tris (3 : 1) (open) ligand–metal complexes for three different oligomer concentrations, respectively. The vertical dashed lines correspond to $r = 0.67$ (stoichiometric composition) and $r = 1.0$.

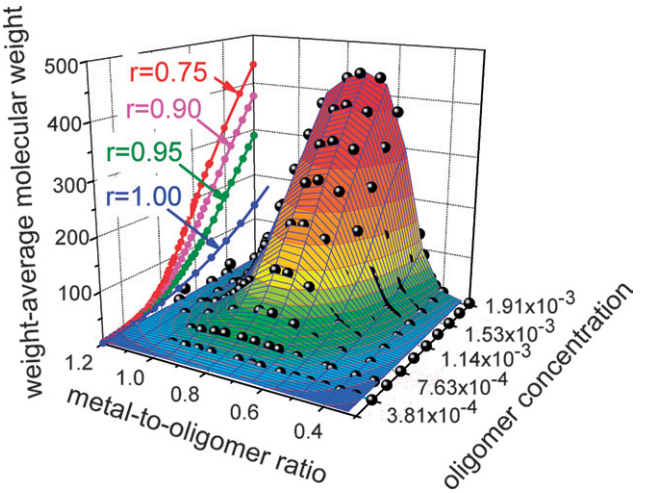

Fig. 7 The composition and oligomer concentration dependence of weight-average molecular weight (in units of oligomer molecular weight). The oligomer concentration dependence of the weight-average molecular weight for several metal-to-oligomer ratios is illustrated as projections.

the range of oligomer concentrations considered and it was also observed in our simulations for a longer oligomer length ($N = 16$, data not shown). At low oligomer concentrations the behavior of the number-average (and to some extent the weight-average) molecular weight is rather asymmetric, *i.e.* its decrease is more pronounced in the metal-rich area (compared to the oligomer-rich region). Around the metal-to-oligomer ratio of 1.0 a shoulder is clearly seen and starts to disappear when the oligomer concentration is increased. The reason for the occurrence of the shoulder at low oligomer concentrations is the strong tendency of oligomers to form intra-molecular bonds, especially in the form of the smallest rings at $r = 1$ (see Fig. 3 and 6). Formation of intra-molecular bonds increases the total number of species and thus results in a decrease in the number-average (and weight-average) molecular weight. Upon close inspection of Fig. 5, it can also be seen that starting from the lowest oligomer concentration considered, the maxima of the weight- and number- average molecular weights shift to slightly larger metal-to-oligomer ratios with increasing oligomer concentrations. A similar shift of the maximum of the reduced viscosity is also observed experimentally for aqueous solutions of Nd^{3+} (or La^{3+}) with bifunctional ligands.[5] As is seen from Fig. 6 the contribution of the smallest rings to the overall polymer population decreases with an increase in oligomer concentration and as a result the appearance of the shoulder at $r = 1$ diminishes and the corresponding molecular weight increases. This shifts the weight-average molecular weight to higher r. A somewhat similar effect was observed experimentally for the viscosity of 2 : 1 metal–ligand complexes.[51,50]

As is seen from Fig. 5, an increase in oligomer concentration results in an increase in the weight- and number-average molecular weights. The concentration dependence of the weight-average molecular weight at different metal-to-oligomer ratios is shown in Fig. 7. A steep increase in M_w is observed above some critical oligomer concentration, which varies with metal-to-oligomer ratio. Similar behavior was observed in computer simulations of the random polycondensation of telechelic linear chains cured with tri- and tetrafunctional crosslinkers.[27] As is seen from the 2-D projection (shown in Fig. 7), the concentration dependence of the weight-average molecular weight increases sharply above some point, exhibiting a sigmoidal profile in the log–log scale with an inflection point corresponding to the onset of reversible network formation.[27,54] Qualitatively similar behavior of the viscosity around the gel point was observed for metallo-supramolecular polymers.[5] At high oligomer concentrations the weight-average molecular weight increases in a linear manner with concentration, indicating that nearly all oligomers are incorporated in a reversible network. As is seen from Fig. 7, for $r \simeq 0.75$, M_w starts to increase at a lower oligomer concentration compared to other metal-to-oligomer ratios. We can recall that $r \simeq 0.75$ corresponds to the metal-to-oligomer ratio when the maximum of M_w is achieved (at least at low oligomer concentrations) (Fig. 5). Away from the stoichiometric composition, the increase in molecular weight with concentration becomes noticeably smaller as the association is limited either by the number of metal ions or oligomers.

3.4 Reversible network formation

As is seen from Fig. 7, above some oligomer concentration the weight-average molecular weight increases rapidly with oligomer concentration for a range of metal-to-oligomer ratios. Also the molecular weight distribution above a certain oligomer concentration starts to exhibit an additional peak indicating formation of large supramolecular objects in the system (Fig. 4). Both of these features are indications of reversible network formation. One can recall that in classical gelation theory[36,54] the sharp increase of weight-average molecular weight accompanies the transition from viscous fluid to elastic gel.

In order to determine the critical conditions (in terms of oligomer concentration and metal-to-oligomer ratio) for reversible network formation, we analyzed the reduced averaged cluster size which is defined as[55]

$$I_{av} = \frac{\sum_i N_i M_i^2 - M_{max}^2}{\sum_i N_i M_i} \quad (7)$$

The reduced averaged cluster size is similar to the weight-average molecular weight, except for subtraction of the contribution of the largest supramolecular species M_{max}. Since M_{max} is rather small at low oligomer concentrations, the reduced averaged cluster size behaves similarly to the weight-average molecular weight, *i.e.* it increases with an increase in oligomer concentration (for fixed metal-to-oligomer ratios) until the onset of reversible network formation (if any). Beyond this point, the contribution of the largest supramolecular species to the weight-average molecular weight rapidly increases, resulting in the sharp decline of the reduced averaged cluster size with further increase in oligomer concentration. Therefore, the maximum of the reduced averaged cluster size represents a clear indication of the onset of reversible network formation,[27,29,55] as shown in Fig. 8.

Another way to obtain the critical conditions for reversible network formation is by analyzing the molecular weight distribution. As is seen from Fig. 4 for the stoichiometric composition, with an increase in oligomer concentration the molecular weight distribution changes from pure exponential decay to a more complex form. The concentration ($c = 8.0 \times 10^{-4}$ for $r = 2/3$) at which the distribution starts to develop an additional peak at larger molecular weights can be considered as a turning point, above which the large molecular weight species (network) starts to grow. Mathematically this point can be found by calculating the slope of the molecular weight distribution and equating it to zero for a finite molecular weight. At oligomer concentrations slightly below the onset of reversible network formation the slope of the molecular weight distribution is negative and exhibits a maximum and a minimum. The point at which the maximum of the slope reaches zero can be taken as the onset of network formation (see ESI†). As is shown in Fig. 8 this definition provides results which are very close to that determined using the reduced averaged cluster size criterion.

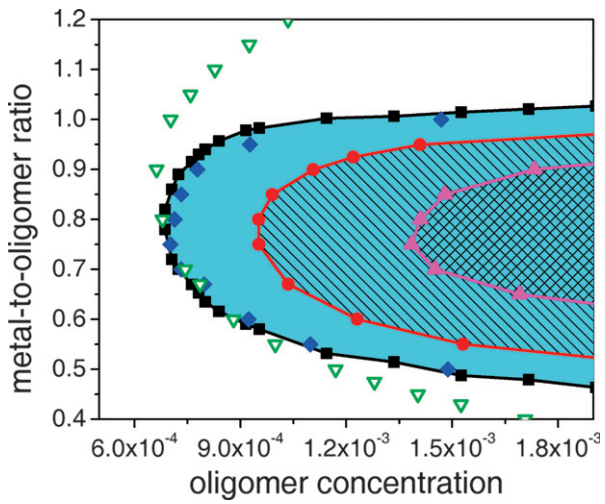

Fig. 8 The critical conditions in terms of metal-to-oligomer ratio and oligomer concentration for: (1) the reversible network formation determined by averaged reduced cluster size (black squares), molecular weight distribution (blue diamonds), (2) the overlap concentration (open triangles), (3) the fraction of sol is equal to that of network (red circles), (4) the fraction of dangling parts being equal to network core (magenta triangles).

As is seen from Fig. 8, reversible network formation requires a sufficient concentration of oligomers and a reasonable balance between the number of oligomers and metal ions. The lowest concentration for the formation of the network ($c = 7.0 \times 10^{-4}$) corresponds to a metal-to-oligomer ratio of about 0.75, where the weight-average molecular weight reaches its maximum as shown in Fig. 5. For other metal-to-oligomer ratios, it takes a larger concentration of oligomers to reach the onset of reversible network formation. As a result, outside of the filled region shown in Fig. 8 ($0.45 \lesssim r \lesssim 1.025$) the small number of oligomers or the mismatch between the number of metal ions and oligomers hinders formation of the network. In the metal-poor region the significant fraction of unreacted oligomers (Fig. 3) prevents formation of the network despite the high fraction of tris (3 : 1) ligand–metal complexes (Fig. 2). Similarly, in the metal-rich regime the dominance of mono (1 : 1) ligand–metal complexes (Fig. 2) leads to formation of short linear chains (Fig. 3) preventing the network formation. This implies that at sufficiently high oligomer concentrations an increase (or decrease) in the metal-to-oligomer ratio can lead to a network formation starting at some metal-to-oligomer ratio r_{low} (r_{high}) below (above) the stoichiometric composition. (Correspondingly the reduced averaged cluster size exhibits two maxima at r_{low} and r_{high} with a minimum in between.) The range of compositions allowing reversible network formation increases with oligomer concentration, especially in the metal-poor region (Fig. 8).

It is worthwhile to compare the onset of the reversible network formation with the overlap concentration, when individual coils formed by reversibly associated (branched) chains and rings start to interpenetrate each other. To evaluate the overlap concentration, we estimated the volume of each individual species as $4\pi < R_g^2 >^{3/2}/3$ (where R_g is the radius of gyration) and equated the sum of volumes for all species to the total volume of the system. By averaging over 4.2×10^6 MCts following equilibration we obtained the overlap concentration (for each metal-to-oligomer ratio), shown in Fig. 8. As is seen in the range of metal-to-oligomer ratios $0.6 \lesssim r \lesssim 0.8$ the overlap concentration practically coincides with the critical concentration for reversible network formation, *i.e.* formation of the network starts as soon as reversibly associated chains/rings begin to interpenetrate each other. At higher or lower metal-to-oligomer ratios the onset of reversible network formation occurs at higher oligomer concentrations when individual polymer coils already overlap each other. The larger oligomer concentration is required to achieve the necessary degree of crosslinking (high r) or large enough overall size of individual branched molecules (small r) to form the network.

Besides the above-mentioned criteria for the onset of network formation, there are a few others which have been applied as indicators of gel formation.[27,30,54,56,57] Among such criteria are the direct percolation method[30,57] when a large structure connecting all sides of the simulation box can be viewed as a gel. In our simulations we found this method to be less precise (compared to the reduced average cluster size and molecular weight distribution) as the results exhibited noticeable fluctuations and were influenced by the box size. One more definition of the gel point which has some practical implications (*e.g.* experimentally

measured viscosity behavior) concerns the abrupt increase in the weight-average molecular weight,[27,54] which we observed in our simulations (Fig. 7). However its practical realization (*e.g.* determination of the inflection point of M_w in a log–log plot) was also somewhat unsatisfactory, as the results were influenced by the choice of oligomer concentration range for fitting and simulation data uncertainty. Instead we considered some molecular interpretations of such criteria. Evidently, beyond the point where the weight fraction of reversible network starts to dominate over the sol fraction, the properties of the network will dominate and one can expect to observe experimentally "gel-like" behavior (*e.g.* based on viscosity measurements). The corresponding range (of oligomer concentrations and metal-to-oligomer ratios) is shown in Fig. 8 (single-hatched area). The points where the weight fraction of network and sol are equal follow the similar general pattern as for the onset of network formation, but are shifted to higher oligomer concentrations. This shift is especially large away from the stoichiometric composition where network growth occurs more gradually. The region between the onset of network formation and the network-dominated area boundary corresponds to the initial stage of network growth when more than one large supramolecular species can compete for dominance and the growth occurs by incorporation of some of the sol molecules into the network (as will be discussed below). A sharp increase in the weight-average molecular weight (and corresponding increase in viscosity) occurs in this region, close to the boundary of the network-dominated area (where the fraction of network and sol are equal) especially at metal-to-oligomer ratios away from the stoichiometric composition.

As mentioned in the Introduction, while the field of analytical models for gelation is very broad, most of them deal with irreversible gelation and consider only one or two factors[34,35] influencing the gelation, while in our system unequal reactivity, substitution (cooperativity of binding) effects and ring formation all play an important role. As a result, it comes as no surprise that comparison with the classical Flory–Stockmayer model[36–38] does not provide a satisfactory result: network formation in our simulations occurs at considerably higher oligomer concentrations (nearly 40 times higher for the stoichiometric composition) and more narrow metal-to-oligomer ratios than anticipated by classical gelation models (data not shown).

3.5 Sol, network and its constituents

As we discussed above, beyond the onset of network formation growth of a large supramolecular network(s) spanning the whole system becomes favorable. This does not mean, however, that all the oligomers will immediately become part of the network. There will remain some fraction of small (branched) rings, chains similar to what exists at lower oligomer concentration. These molecules, sol, will coexist in equilibrium with the network. The molecular make-up of the sol is dominated by the same small species as at low oligomer concentration (Fig. 3). At the onset of network formation the fraction of sol is close to 1, as is seen from Fig. 9, where the concentration dependence of the weight fraction of oligomers in the network (network fraction) and sol (sol fraction) are shown for the metal-to-oligomer ratio, $r = 0.75$. With an increase in oligomer concentration the network fraction

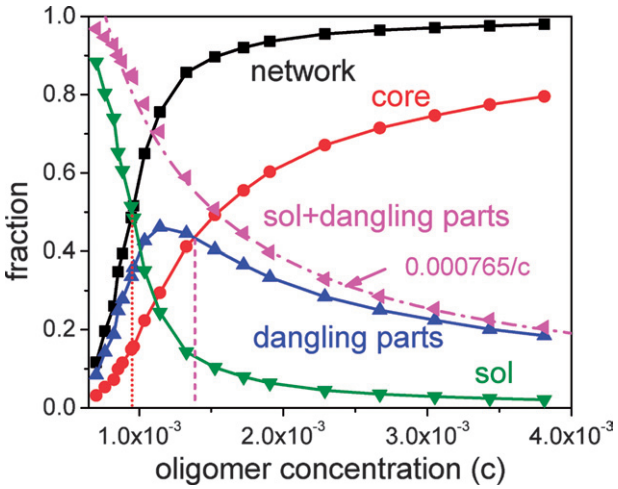

Fig. 9 The oligomer concentration dependence of the fraction of network (black squares), network core (red circles), dangling parts (blue up triangles) and sol (olive down triangles) for $r = 0.75$. The simulation results for the sum of sol and dangling parts are shown as magenta left triangles and the best fit of the data to A/c (see text) is shown as dash–dot curve with the equation used shown next to the curve. The vertical dotted line corresponds to the point where the fraction of sol and network are equal and the vertical dashed line indicates the point where fractions of dangling parts and core are equal. The lowest concentration shown corresponds to the onset of network formation.

increases rapidly until it levels off, gradually reaching unity. At this point the weight-average molecular weight approaches the total number of oligomers in the system. The growth of the network occurs at the expense of the sol, whose fraction decreases with an increase in the oligomer concentration, tending to zero at higher concentrations. For metal-to-oligomer ratios away from the stoichiometric composition, *e.g.* $r = 0.5$, the growth of the network fraction (and decline of the sol fraction) occurs more slowly with concentration, leveling off at some value less than 1 (about 0.8 for $r = 0.5$) implying the existence of a significant fraction of sol even at the highest oligomer concentrations. This is a consequence of the mismatch between the number of metal sites and ligands, resulting in some fraction of ligands or metal sites remaining unoccupied within the molecules contributing to the sol.

To get an insight into the architecture of the metallo-supramolecular network, we analyzed our simulation results distinguishing between the core (the highly-crosslinked part of the network) and the dangling parts. We define the dangling parts as the branches of the network which are connected to the rest of the network through a single path, *i.e.* cutting this path would lead to the formation of separate independent species. Dangling parts include rings, linear and branched chains connected by one end to the rest of the network. The concentration dependence of the weight fraction of dangling parts and network core (with respect to the total amount of oligomers in the system) is shown in Fig. 9 for $r = 0.75$. As is seen, close to the onset of network formation the weight fraction of dangling parts exceeds that of the core. With a further increase in oligomer concentration the fraction of core consistently increases while the fraction of dangling parts firstly increases and exhibits

a maximum followed by a decrease. As a result, above a certain oligomer concentration the core fraction starts to exceed the dangling part contribution. One can recall that dangling parts do not carry stress[36,58] so this oligomer concentration can be considered as the boundary of an "elastic network". The corresponding concentrations (when the fraction of core and dangling parts become equal) are shown in Fig. 8. As is seen, this concentration is noticeably higher than the concentration when the number of oligomers in the network starts to dominate that in the sol and the range of metal-to-oligomer ratios is more narrow. The latter observation is connected with the fact that the larger is the mismatch between the number of ligands and metal sites, the larger is the weight fraction of dangling parts and it takes a larger oligomer concentration for the weight fraction of the core to reach that for dangling parts. For a range of metal-to-oligomer ratios away from stoichiometric composition (especially in the metal-rich region) the weight fraction of the core never exceeds that of the dangling parts.

While analyzing the properties of the network and sol in the range $0.65 \lesssim r \lesssim 0.9$, one can make an interesting observation. In this range the decrease in the number of oligomers in the sol with an increase in concentration beyond the onset of network formation is accompanied by nearly the same increase in the number of oligomers that associated with the dangling parts. To illustrate this point we plotted in Fig. 9 the weight fraction of oligomers in the sol and the dangling parts together and fitted it by A/c function (noting that the simulation volume is constant, an increase in oligomer concentration c would imply a decrease in weight fraction of a constant according to a reciprocal function). As is seen the fit is rather good with the constant, $A = 7.65 \times 10^{-4}$, being close to the concentration of oligomers at the onset of network formation for $r = 0.75$. This behavior implies that at concentrations just above the onset of network formation some fraction of sol molecules become incorporated into the network as dangling parts. When the number of oligomers in the sol becomes smaller at higher concentration (*i.e.* the network-dominated regime), this mechanism of network growth becomes inactive and the weight fraction of dangling parts starts to decline. Even through the absolute number of oligomers in the dangling parts may slowly increase with concentration the maximum number is limited by the number of oligomers at the onset of network formation. This implies that there is a critical mass of oligomers necessary to start the network formation process and this number of oligomers remains practically constant in the form of sol or dangling parts of the network throughout the whole oligomer concentration range considered herein. In other words, almost any additional oligomer in excess of the amount corresponding to the onset of network formation will contribute to the core of the growing network while the number of oligomers in the sol and dangling parts remains nearly constant. While this observation holds in the range $0.65 \lesssim r \lesssim 0.9$, where the fraction of dangling parts becomes rather small at high oligomer concentrations, outside this range the number of oligomers in dangling parts grows continuously without leveling off and the fraction of oligomers in the sol does not decrease as much. As we discussed above, a strong mismatch between the number of ligands and metal ions implies a large or even dominant fraction of dangling parts in the network indicating possibly a different mechanism of network growth and resulting in a supramolecular network with different properties (*e.g.* elastic properties, see next section).

3.6 Mesh size and elastic modulus

Another important characteristic of the network is the degree of crosslinking or average mesh size. In our system only tris (3 : 1) ligand–metal complexes can serve as crosslinks. According to Scanlan[59] and Case,[60] the effective crosslinks are those with at least three paths to the rest of the network. Therefore among tris (3 : 1) ligand–metal complexes only those which are not part of dangling branches (or serve as the attachment points for dangling parts) will be effective crosslinks. The number of effective crosslinks, N_x, can be directly obtained from the simulations (as long as the dangling parts are determined). The strand of (several) oligomers connected at both ends to the effective crosslinks can carry stress and can be considered elastically active. Knowing the number of effective crosslinks N_x, the number of elastically active strands is simply $N_s = 3N_x/2$ (as each metal ion in 3 : 1 complexes is connected to 3 ligands and there are two ligands per oligomer). The bis (2 : 1) ligand–metal complexes merely extend the length of an elastically active strand. Thus the average molecular weight between effective crosslinks (in units of oligomer mass) is $M_e = (N_n - N_d)/N_s$, where N_n and N_d are the number of oligomers in the network and dangling parts, respectively.

The average molecular weight between effective crosslinks has been calculated for different oligomer concentrations and metal-to-oligomer ratios and the results are shown in Fig. 10. The average molecular weight between effective crosslinks M_e decreases with an increase in metal content, reaches a minimum around the stoichiometric composition and then increases with a further increase in metal content. As is seen from Fig. 10, these changes are relatively symmetric with respect to the composition

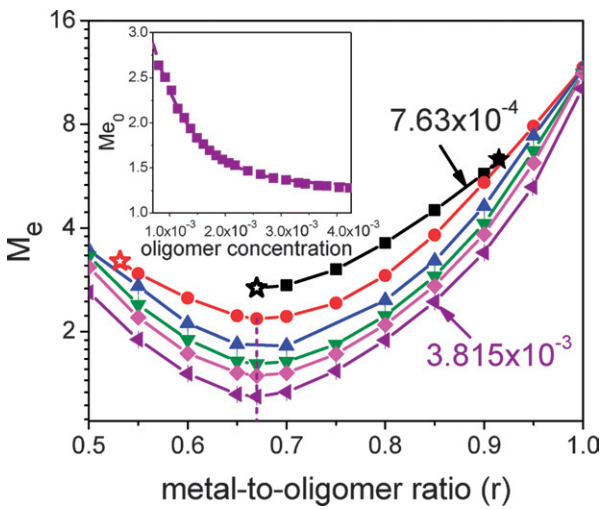

Fig. 10 The composition dependence of the average molecular weight between effective crosslinks M_e for different oligomer concentrations ($c = 7.63 \times 10^{-4}$, $c = 1.14 \times 10^{-3}$, $c = 1.53 \times 10^{-3}$, $c = 1.9 \times 10^{-3}$, $c = 2.3 \times 10^{-3}$, and $c = 3.8 \times 10^{-3}$ from top to bottom). The minimum of M_e occurs at the stoichiometric composition for all concentrations (dashed line). The inset shows the concentration dependence of the minimum molecular weight between effective crosslinks M_{e0} (see text).

corresponding to the minimum of M_e (at least in the range $0.55 < r < 0.90$). By fitting the data for a constant oligomer concentration [using the equation $M_e = A(r - r_0)^2 + M_{e0}$] the minimum of the molecular weight between effective crosslinks (M_{e0}) was determined to be at the stoichiometric composition $r_0 = 2/3$ (within the simulation error bar). Comparing results for different oligomer concentrations we found that M_{e0} decreases systematically with an increase in oligomer concentration (as shown in the inset of Fig. 10) reaching values as small as 1.3 times the oligomer weight. In the metal-rich cases ($r > 0.9$) M_e can reach noticeably larger values (up to 12 oligomer weights) which is consistent with the larger fraction of bis (2 : 1) ligand–metal complexes in this area. For a fixed metal-to-oligomer ratio, the molecular weight between effective crosslinks decreases with an increase in oligomer concentration, following a qualitatively similar trend as for M_{e0}. Similar behavior was experimentally observed for neodymium(III)-2,6-dicarboxypyridine ligand gels (based on the behavior of the measured elastic modulus).[6]

We have also calculated the average mesh size of the network, r_m, *i.e.* the average distance between effective crosslinks (details of the calculations are described in the ESI†). We found that mesh size varies in the range $11a \lesssim r_m \lesssim 36a$ and follows a somewhat weaker overall dependence $r_m \sim M_e^{0.475}$ than the end-to-end distance $R_{end} \sim M^{0.63}$ (where M is the molecular weight) of a linear chain in dilute solution (see Fig. S2 in the ESI†). This is likely the result of high average density of the network core.

The elastic response of the reversible polymer network to a deformation can be characterized by the equilibrium high-frequency elastic plateau modulus G_0.[6] An estimation of G_0 can be made assuming that the elasticity is mainly supported by the effective strands of the network, N_s, which contribute to the macroscopic elastic response as:

$$G_0 \cong N_s kT \tag{8}$$

Besides the contribution of effective strands, the plateau modulus G_0 can also be influenced by entanglement effects.[61] For irreversible polymer networks and melts studied using the BFM approach (similar to what we use) it was shown that entanglements start to play an important role in the dynamic (and elastic) properties of the system for chain lengths higher than 38 monomers.[62,63] Since we use oligomers of much shorter length (6 spacer monomers with two terminal ligands) and consider reversible crosslinking (or branching) the entanglement effects are expected to be very minor compared to the contribution of the effective strands to G_0 and will be ignored below. We note that we define G_0 in terms of the absolute values of the number of effective strands rather than their concentration[30,36] which does not affect the concentration dependence of G_0, taking into account that the volume of the simulation box is fixed.

The contour plot of G_0 on the plane of metal-to-oligomer ratio and oligomer concentration is shown in Fig. 11. As expected G_0 increases with an increase in oligomer concentration reaching its maximum around the stoichiometric composition, where the molecular weight between effective crosslinks M_e is found to be the smallest (Fig. 10). At lower oligomer concentrations the largest values of G_0 are attained at a somewhat larger metal-to-oligomer ratio, $r \simeq 0.7$, where the weight-average molecular

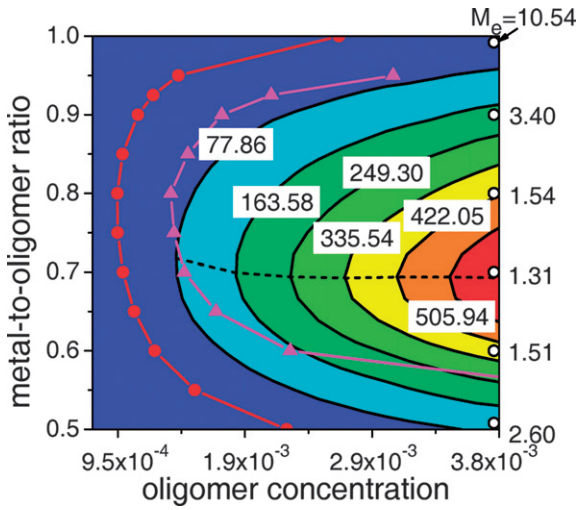

Fig. 11 A contour plot of G_0 (in units of kT, labeled on each curve) on the plane of metal-to-oligomer ratio and oligomer concentration. The red circles and magenta triangles are the same as in Fig. 8 and correspond to the points when the sol fraction is equal to the network fraction and the core fraction is equal to that for the dangling parts. The dashed line connects the metal-to-oligomer ratios at which the maximum of the G_0 occurs for any given oligomer concentration. The average molecular weight between effective crosslinks (in units of oligimer molecular weight) is shown on the right at the oligomer concentration 3.8×10^{-3} for several metal-to-oligomer ratios.

weight is large (Fig. 7). In contrast to M_e discussed above, G_0 is asymmetric with respect to the stoichiometric composition: for the same value of M_e, G_0 is higher in the metal-rich region compared to the metal-poor region (Fig. 11). This trend can be understood taking into account that while in the metal-rich region the overall fraction of 3 : 1 complexes is low, a considerable fraction of them serve as effective crosslinks N_x. In contrast, the large number of tris (3 : 1) ligand–metal complexes in the metal-poor region (Fig. 2) does not result in a significant number of effective crosslinks, as a large number of sol species and highly branched dangling parts consume a large fraction of 3 : 1 complexes. Comparing the boundary of the "elastic network" (*i.e.* where the fraction of the core equals that of dangling parts) with constant G_0 lines one can notice that the latter is slightly shifted to lower r values (especially in metal-poor region). The main reason for this is that G_0 is calculated based on the absolute number of effective crosslinks (which is largest near the stoichiometric composition) while the "elastic network" boundary is defined based on weight fractions (with a maximum in the weight-average molecular weight attained around $r \simeq 0.75$, Fig. 5 and 7).

The concentration dependence of the high-frequency elastic plateau modulus G_0 is presented in Fig. 12 for a range of metal-to-oligomer ratios in the "elastic network" region. Besides the general increase in G_0 with concentration, one can notice that quantitatively the behavior of G_0 is rather similar for all r considered, especially at high oligomer concentrations. In particular, a similar scaling dependence can be noticed (in the log–log scale of Fig. 12) at large oligomer concentrations:

$$G_0 \sim c^{1.8} \tag{9}$$

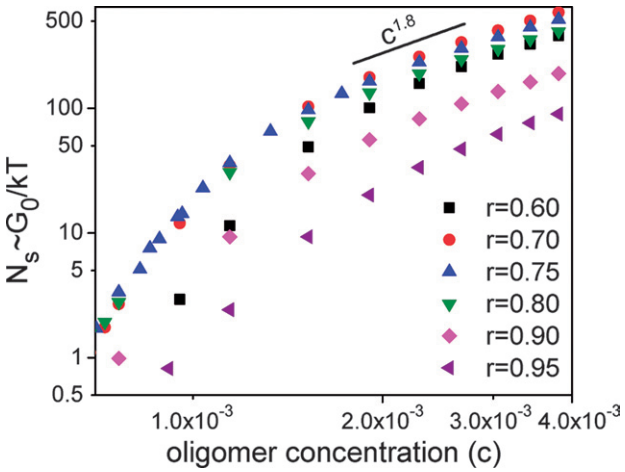

Fig. 12 The oligomer concentration dependence of G_0/kT for several metal-to-oligomer ratios. At higher concentrations G_0/kT follows a $c^{1.8}$ dependence shown by the solid line.

It is interesting to note that the same scaling dependence was observed for neodymium(III)-2,6-dicarboxy-pyridine ligand supramolecular networks (for C6 oligomers).[6] Earlier a similar dependence was reported for branched worm-like CTAB (hexadecyltrimethylammonium bromide) micelles (in the presence of a large concentration of salt).[15] While this dependence is somewhat weaker than what is expected for networks in the semidilute regime,[58] $c^{9/4}$, it is plausible that this scaling is a reflection of the common mechanism of elastic response in these types of reversible networks including breaking and reformation of bonds in a new place without changing the degree of association. We note that for r values outside the range given in Fig. 12 not only is G_0 smaller (Fig. 11) but it also follows a qualitatively different c dependence, that reflects a different network architecture (*e.g.* a large fraction of dangling parts compared to the core).

The results presented above are based on the series of simulations performed for constant values of association energies for the first, second and third ligand–metal bond and a flexible spacer of 6 repeat units. Evidently the association energy, spacer length and flexibility can all influence the obtained results because of the complex interplay of these factors. For instance, increasing the spacer length and rigidity would decrease the probability of (monomolecular) ring formation.[32,52] As a result one can expect preferential formation of branched molecules of larger molecular weight and network formation at lower oligomer concentrations. These factors may also influence the metal-to-oligomer ratio corresponding to the maximum of molecular weight, elastic plateau modulus or network fraction.[28] Clearly, formation of metallo-supramolecular networks is a complicated process, influenced by a range of parameters. It would be desirable to develop an analytical approach that describes the behavior of metallo-supramolecular networks, which will be a subject of our future work.

4 Conclusions

In this paper we have applied Monte Carlo simulations and an analytical approach to study metal–ligand complexation in solution at thermodynamic equilibrium. The metal ions could form complexes with up to three ligands, leading to a reversible metallo-supramolecular network under certain conditions. We have investigated the effects of oligomer concentration and metal-to-oligomer ratio on the formation and the properties of the metallo-supramolecular network.

We found that for a constant oligomer concentration in the oligomer-rich region tris (3 : 1) ligand–metal complexes dominate. Their fraction decreases with an increase in the metal content giving rise to bis (2 : 1) ligand–metal complexes (with a maximum around $r = 1$) and mono (1 : 1) ligand–metal complexes (with a maximum at $r = 2$). These simulation results favorably compare with a chemical-equilibrium based analytical model (Fig. 2). The influence of oligomer concentration on the fraction of different ligand–metal complexes is noticeable mainly in the oligomer-rich region: the fraction of 2 : 1 and 1 : 1 ligand–metal complexes decreases and the fraction of tris (3 : 1) ligand–metal complexes increases with an increase in oligomer concentration. For $r = 1$ ring formation is strongly preferable at low concentrations giving rise to 2 : 1 ligand–metal complexes. The population of the most favorable small species as a function of metal-to-oligomer ratio was analyzed (Fig. 3).

Our analysis shows that the weight fraction decays exponentially with molecular weight at low oligomer concentration, as expected. At higher oligomer concentration the molecular weight distribution exhibits a maximum at high molecular weights indicating network formation (Fig. 4). For a constant low oligomer concentration, the number-average molecular weight reaches its maximum at the stoichiometric composition ($r = 2/3$), while the maximum position for the weight-average molecular weight is achieved at a somewhat higher metal-to-oligomer ratio, $r = 0.75$ when there is a significant fraction of both 2 : 1 and 3 : 1 ligand–metal complexes (Fig. 5). We found that with an increase in oligomer concentration the maximum positions for both M_n and M_w shift to larger metal-to-oligomer ratios, in agreement with reduced viscosity measurements for aqueous solutions of Nd^{3+} (or La^{3+}) with bifunctional ligands terminated by pyridine-2,6-dicarboxylate groups.[5] We explained this shift based on the decrease in the fraction of the smallest rings and hence increase of molecular weight at $r = 1$ (Fig. 6).

The onset of reversible network formation was determined in our simulations by analyzing the reduced averaged cluster size and molecular weight distribution. It was found that the formation of metallo-supramolecular networks starts at low concentration in the range of metal-to-oligomer ratios close to $r = 0.75$, where the weight-average molecular weight reaches its maximum. With an increase in oligomer concentration network formation expands to a range of metal-to-oligomer ratios, with critical values r_{upper} and r_{lower} above or below which a network will never form due to the strong mismatch between the number of oligomers and metal ions (Fig. 8). Another measure of network formation, which is relevant to the experimentally measured viscosity, can be defined as the point above which the network fraction dominates over the sol fraction. The range of corresponding metal-to-oligomer ratios is even more narrow in this case compared to the onset of network formation and is shifted to higher concentrations (Fig. 8).

Analyzing the network properties, we found that at oligomer concentrations slightly above the onset of network formation,

network growth proceeds *via* incorporation of sol molecules into the network in the form of dangling parts. At higher concentrations this mechanism of network growth becomes inactive and the fraction of dangling parts starts to decrease together with the sol fraction (Fig. 9). We noticed that the overall number of oligomers in the sol and dangling parts often remains constant over a range of concentrations and is approximately equal to the total amount of oligomers at the onset of network formation. We also analyzed the oligomer concentration and metal-to-oligomer ratio dependence of the average molecular weight M_e between effective crosslinks (*i.e.* the crosslinks carrying stress). We found that M_e decreases with an increase in concentration in a qualitatively similar manner as was experimentally observed,[6] with the smallest M_e achieved at the stoichiometric composition (Fig. 10). Correspondingly, the high-frequency elastic plateau modulus G_0 also reaches its largest values near the stoichiometric composition at high concentration. At lower oligomer concentrations the maximum in G_0 shifts more towards $r = 0.75$, *i.e.* the maximum in the weight-average molecular weight. Analyzing the concentration dependence of the elastic plateau modulus for $0.60 \leq r \leq 0.95$ we found that it follows $G_0 \sim c^{1.8}$ scaling dependence (in the high oligomer concentration range), similar to the experimental observations for neodymium(III)-2,6-dicarboxypyridine ligand supramolecular networks (for C6 oligomers)[6] and branched worm-like CTAB micelles (in the presence of a high concentration of salt).[15]

Acknowledgements

We thank S. J. Rowan for helpful discussions. This material is based upon work supported by the National Science Foundation under Grant No. 0348302.

References

1 A. Ciferri, *Supramolecular Polymers*, CRC Press, Boca Raton, FL, 2nd edn, 2005.
2 U. S. Schubert and C. Eschbaumer, *Angew. Chem., Int. Ed.*, 2002, **41**, 2893–2926.
3 J. M. Lehn, *Polym. Int.*, 2002, **51**, 825–839.
4 J. B. Beck and S. J. Rowan, *J. Am. Chem. Soc.*, 2003, **125**, 13922–13923.
5 T. Vermonden, W. M. de Vos, A. T. M. Marcelis and E. J. R. Sudholter, *Eur. J. Inorg. Chem.*, 2004, **2004**, 2847–2852.
6 T. Vermonden, M. J. van Steenbergen, N. A. M. Besseling, A. T. M. Marcelis, W. E. Hennink, E. J. R. Sudholter and M. A. Cohen Stuart, *J. Am. Chem. Soc.*, 2004, **126**, 15802–15808.
7 Y. Q. Zhao, J. B. Beck, S. J. Rowan and A. M. Jamieson, *Macromolecules*, 2004, **37**, 3529–3531.
8 W. G. Weng, J. B. Beck, A. M. Jamieson and S. J. Rowan, *J. Am. Chem. Soc.*, 2006, **128**, 11663–11672.
9 D. M. Loveless, S. L. Jeon and S. L. Craig, *Macromolecules*, 2005, **38**, 10171–10177.
10 D. M. Loveless, S. L. Jeon and S. L. Craig, *J. Mater. Chem.*, 2007, **17**, 56–61.
11 W. C. Yount, D. M. Loveless and S. L. Craig, *J. Am. Chem. Soc.*, 2005, **127**, 14488–14496.
12 R. Dobrawa and F. Wurthner, *J. Polym. Sci., Part A: Polym. Chem.*, 2005, **43**, 4981–4995.
13 D. G. Kurth and M. Higuchi, *Soft Matter*, 2006, **2**, 915–927.
14 M. E. Cates and S. J. Candau, *J. Phys.: Condens. Matter*, 1990, **2**, 6869–6892.
15 A. Khatory, F. Lequeux, F. Kern and S. J. Candau, *Langmuir*, 1993, **9**, 1456–1464.
16 S. J. Rowan and J. B. Beck, *Faraday Discuss.*, 2005, **128**, 43–53.
17 J. M. J. Paulusse, J. P. J. Huijbers and R. P. Sijbesma, *Macromolecules*, 2005, **38**, 6290–6298.
18 J. M. J. Paulusse, D. J. M. van Beek and R. P. Sijbesma, *J. Am. Chem. Soc.*, 2007, **129**, 2392–2397.
19 R. F. M. Lange, M. Van Gurp and E. W. Meijer, *J. Polym. Sci., Part A: Polym. Chem.*, 1999, **37**, 3657–3670.
20 V. Berl, M. Schmutz, M. J. Krische, R. G. Khoury and J. M. Lehn, *Chem.–Eur. J.*, 2002, **8**, 1227–1244.
21 Y. Chujo, K. Sada and T. Saegusa, *Macromolecules*, 1993, **26**, 6315–6319.
22 Y. Chujo, K. Sada and T. Saegusa, *Macromolecules*, 1993, **26**, 6320–6323.
23 S. Schmatloch and U. S. Schubert, *Macromol. Symp.*, 2003, **199**, 483–497.
24 G. N. Tew, K. A. Aamer and R. Shunmugam, *Polymer*, 2005, **46**, 8440–8447.
25 W. H. Binder and R. Zirbs, *Adv. Polym. Sci.*, 2007, **207**, 1–78.
26 Y. K. Leung and B. E. Eichinger, *J. Chem. Phys.*, 1984, **80**, 3877–3884.
27 L. Y. Shy, Y. K. Leung and B. E. Eichinger, *Macromolecules*, 1985, **18**, 983–986.
28 N. Gilra, C. Cohen and A. Z. Panagiotopoulos, *J. Chem. Phys.*, 2000, **112**, 6910–6916.
29 A. G. Balabanyan, E. Y. Kramarenko, I. A. Ronova and A. R. Khokhlov, *Polymer*, 2005, **46**, 4248–4257.
30 M. Nguyenmisra and W. L. Mattice, *Macromolecules*, 1995, **28**, 1444–1457.
31 R. D. Groot and W. G. M. Agterof, *J. Chem. Phys.*, 1994, **100**, 1649–1656.
32 C. Chen and E. E. Dormidontova, *J. Am. Chem. Soc.*, 2004, **126**, 14972–14978.
33 M. Gordon and G. R. Scantlebury, *J. Chem. Soc. B*, 1967, 1–13.
34 L. J. Kasehagen, S. E. Rankin, A. V. McCormick and C. W. Macosko, *Macromolecules*, 1997, **30**, 3921–3929.
35 S. Pereda, A. Brandolin, E. M. Valles and C. Sarmoria, *Macromolecules*, 2001, **34**, 4390–4400.
36 P. J. Flory, *Principles of Polymer Chemistry*, Cornell University Press, Ithaca, New York, 1953.
37 W. H. Stockmayer, *J. Chem. Phys.*, 1943, **11**, 45–55.
38 W. H. Stockmayer, *J. Chem. Phys.*, 1944, **12**, 125–131.
39 P. D. Gujrati, *J. Phys. A: Math. Gen.*, 2001, **34**, 9211–9230.
40 R. Miller and C. W. Macosko, *Macromolecules*, 1978, **11**, 656–662.
41 H. Rolfes and R. F. T. Stepto, *Makromol. Chem., Macromol. Symp.*, 1993, **76**, 1–12.
42 J. T. Kindt, *J. Phys. Chem. B*, 2002, **106**, 8223–8232.
43 M. Lang, D. Goritz and S. Kreitmeier, *Macromolecules*, 2005, **38**, 2515–2523, and references therein.
44 D. R. Miller and C. W. Macosko, *Macromolecules*, 1980, **13**, 1063–1069.
45 I. Carmesin and K. Kremer, *Macromolecules*, 1988, **21**, 2819–2823.
46 H. P. Deutsch and K. Binder, *J. Chem. Phys.*, 1991, **94**, 2294–2304.
47 *Metal-Containing Polymeric Materials*, ed. C. U. Pittman, J. M. Z. Carraher, J. E. Sheats and B. M. Culbertson, Plenum Press, NY, 1996.
48 I. Grenthe, *J. Am. Chem. Soc.*, 1961, **83**, 360–364.
49 J. P. Wittmer, A. Milchev and M. E. Cates, *J. Chem. Phys.*, 1998, **109**, 834–845.
50 J. van der Gucht, N. A. M. Besseling and H. P. van Leeuwen, *J. Phys. Chem. B*, 2004, **108**, 2531–2539.
51 T. Vermonden, J. van der Gucht, P. de Waard, A. T. M. Marcelis, N. A. M. Besseling, E. J. R. Sudholter, G. J. Fleer and M. A. Cohen Stuart, *Macromolecules*, 2003, **36**, 7035–7044.
52 M. C. Hagy, C. C. Chen and E. E. Dormidontova, *Macromolecules*, 2007, **40**, 3408–3421.
53 M. K. Nazeeruddin, S. M. Zakeeruddin, R. Humphry-Baker, S. I. Gorelsky, A. B. P. Lever and M. Gratzel, *Coord. Chem. Rev.*, 2000, **208**, 213–225.
54 D. Stauffer, A. Coniglio and M. Adam, *Adv. Polym. Sci.*, 1982, **44**, 103–158.
55 J. Hoshen and R. Kopelman, *Phys. Rev. B*, 1976, **14**, 3438–3445.
56 S. K. Kumar and A. Z. Panagiotopoulos, *Phys. Rev. Lett.*, 1999, **82**, 5060–5063.

57 S. K. Kumar and J. F. Douglas, *Phys. Rev. Lett.*, 2001, **87**(18), 188301–118304.
58 *Scaling Concepts in Polymer Physics*, ed. P.-G. de Gennes, Cornell University Press, Ithaca, NY, 1979.
59 J. Scanlan, *J. Polym. Sci.*, 1960, **43**, 501–508.
60 L. C. Case, *J. Polym. Sci.*, 1960, **45**, 397–404.
61 M. Rubinstein and R. H. Colby, *Polymer Physics*, Oxford University Press, New York, 2003.
62 H. L. Trautenberg, J.-U. Sommer and D. Göritz, *J. Chem. Soc., Faraday Trans.*, 1995, **91**(16), 2649–2653.
63 T. Kreer, J. Baschnagel, M. Müller and K. Binder, *Macromolecules*, 2001, **34**(4), 1105–1117.